Grating-coupled silicon-on-sapphire integrated slot waveguides operating at mid-infrared wavelengths

Yi Zou,[1,*] Harish Subbaraman,[2] Swapnajit Chakravarty,[2,3] Xiaochuan Xu,[2] Amir Hosseini,[2] Wei-Cheng Lai,[1] Parker Wray,[1] and Ray T. Chen[1,4]

[1]*Microelectronics Research Center, Electrical and Computer Engineering Department, University of Texas at Austin, Austin, Texas 78758, USA*

[2]*Omega Optics, Inc., Austin, Texas 78757, USA*

[3]*e-mail: swapnajit.chakravarty@omegaoptics.com*

[4]*e-mail: raychen@uts.cc.utexas.edu*

**Corresponding author: yzou@utexas.edu*

Received March 6, 2014; revised April 20, 2014; accepted April 21, 2014; posted April 22, 2014 (Doc. ID 207777); published May 15, 2014

We demonstrate subwavelength bidirectional grating (SWG) coupled slot waveguide fabricated in silicon-on-sapphire for transverse electric polarized wave operation at 3.4 μm wavelength. Coupling efficiency of 29% for SWG coupler is experimentally achieved. Propagation loss of 11 dB/cm has been experimentally obtained for slot waveguides. Two-step taper mode converters with an insertion loss of 0.13 dB are used to gradually convert the strip waveguide mode into slot waveguide mode.

OCIS codes: (230.7370) Waveguides; (130.3120) Integrated optics devices; (130.3060) Infrared.
http://dx.doi.org/10.1364/OL.39.003070

The mid-infrared (MIR) regime, which typically ranges from 2 to 20 μm, has attracted a lot of interest due to its potential applicability in a wide variety of areas, such as trace-gas sensing, free-space communication, environmental monitoring, and thermal imaging [1].

Most of the chemical bonds have much stronger absorption peaks in MIR than near-infrared (NIR), so by moving from NIR to MIR, the sensitivity of spectroscopy can be enhanced by several orders.

As proposed by Soref [1] and Soref *et al.* [2], silicon is an ideal platform for MIR applications up to 8 μm, benefiting from its low material losses, availability of a mature fabrication technology, and its high refractive index. Traditional silicon on insulator wafer has been widely used in the NIR, but it is limited by high absorption loss of silicon dioxide in the range between 2.6 and 2.9 μm and above 3.5 μm. Hence, silicon on sapphire (SOS) was proposed as an alternative platform that has a transparent window up to 5.5 μm. Additionally, it also provides a high refractive index contrast between the core and the cladding [1,2]. So far, SOS-based strip waveguides operating at 2.75 μm [3], 4.5 μm [4,5], 5.18 μm [6], and 5.5 μm [7] wavelengths have been demonstrated. Besides, several optical components, such as grating couplers operating at 2.75 μm [3,8] and 4.5 μm [5], ring resonators operating at 2.75 μm [8], 4.5 μm [5], and 5.5 μm [7] have been realized on SOS. The SOS platform is thus very attractive for integrated MIR photonics. So far, to the best of our knowledge, slot waveguides have not been demonstrated on SOS platform. Slot waveguides can provide enhanced light-matter interaction and thus are very useful components for both optical sensing to achieve high sensitivity and on-chip interconnects for device miniaturization. The enhanced electric field in the narrow low-index slot in slot waveguides compared to conventional waveguides has already been demonstrated in the NIR [9,10]. The high optical confinement, combined with the inherent larger absorption cross section of fundamental molecular vibration signatures of various organic and inorganic compounds in the MIR, can lead to an effectively more sensitive sensor device.

In this Letter, we demonstrate subwavelength grating (SWG) coupled slot waveguide for the first time in SOS for transverse electric (TE) polarized wave operation at 3.4 μm wavelength.

The slot waveguides are designed using FIMMWAVE software from PhotonDesign. The rail width W and the slot width S are optimized to achieve high confinement in the slot, as shown in Fig 1(a). High electric-field confinement (about 43%) is achieved in the slot for $W = 0.6$ μm and $S = 0.13$ μm. Figure 1(b) shows the TE field profile in the slot waveguide corresponding to the above dimensions.

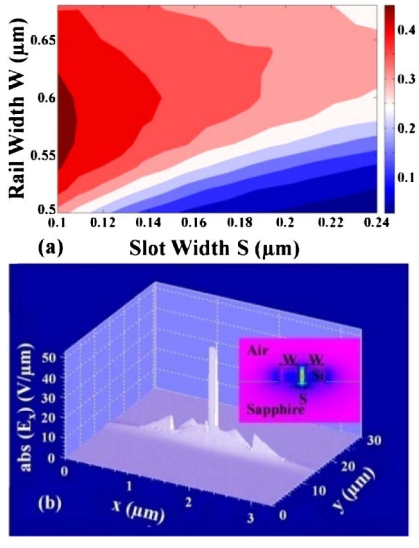

Fig. 1. (a) 2D plot showing simulated confinement factor as a function of slot width S and rail width W. The scale bar on the right indicates confinement factor. (b) Simulated electric field for a slot waveguide with $W = 0.6$ μm and $S = 0.13$ μm. A high confinement in the slot is obtained.

Next, we designed an efficient strip-to-slot waveguide mode converter. A mode converter is a very crucial component in slot waveguide devices. A poorly designed mode converter would lead to large insertion losses. In the NIR, several mode converters have been proposed to achieve highly efficient conversion [11–14]. Two-step tapers have more efficient performance and are more robust to fabrication errors compared to other mode converters in the literature [11–15]. We therefore adopt a two-step taper structure in our design [15]. The structure is shown in Fig. 2(a). A strip waveguide with a width of 1 μm is chosen to ensure single mode propagation of the fundamental TE polarized wave. The mode converter is composed of two sections: a taper 1 section with length $L_{\text{taper1}} = 4$ μm, where the slot width S is reduced from 600 to 130 nm, and a taper 2 section with length $L_{\text{taper2}} = 10$ μm, where the silicon rail width changes from 1 μm to 600 nm, as shown in Fig. 2(a). Taper 1 helps to keep the reflection losses low [15]. Taper 2 ensures that the electric field converts gradually from the strip waveguide into the air gap and finally forms the slot mode.

The above parameters provided the best simulated conversion efficiency of 98% (–0.08 dB) from a set of scans with varying L_{taper1} and L_{taper2} using FIMMWAVE as shown in Fig. 2(b). The electric field distribution for the optimized design is also plotted in Fig. 2(a).

In order to couple light into and out of the waveguide components, SWG couplers are designed, with an operating wavelength at 3.4 μm. The grating couplers are designed based on our previous design procedure [16,17]. TE polarized wave is selected since our vertical slot waveguide only supports TE wave. A 2D simulation package from CAMFR is first utilized to get the optimized period and filling factor along waveguide propagation direction, as well as the effective subwavelength refractive index (n_{sub}). The simulated parameters are then verified using 2D FDTD. Next, the parameters of the subwavelength structure, such as air trench width, length, and period, are calculated by using effective index approximation [18]. For our structure operating at 3.4 μm wavelength, the optimized SWG trench width, length, and period are calculated as 152, 825, and 800 nm, respectively. The grating period is set at 1500 nm. The design results in an effective subwavelength refractive index (n_{sub}) of 2.45 in the propagation direction, and the peak emission angle is obtained at 11° from normal incidence. The simulated transmission spectrum, indicated in red in Fig. 3(a), shows a maximum efficiency of about 36% from fiber to SWG coupler near 3.4 μm. The simulated optical field distribution is shown in Fig. 3(b). It can be seen that good coupling into a fiber positioned at 11° is achieved.

The devices are fabricated on a SOS platform with 600 nm silicon layer on a 500 μm thick sapphire substrate. A 140 nm silicon dioxide layer is first deposited on top of silicon layer using plasma enhanced chemical vapor deposition to serve as a hard mask for pattern transfer. All the components including SWG couplers, strip waveguides, slot waveguides, and strip-to-slot waveguide mode converters are patterned in one step using the JEOL JBX-6000FS electron-beam lithography tool with ZEP-520A e-beam resist, followed by developing in n-Amyl acetate (ZEP-N50) for 2 minutes, and rinsing in isopropyl alcohol. The e-beam resist pattern is next transferred to silicon dioxide by reactive ion etching using CHF_3 and O_2 at 400 V DC bias and 40 mTorr pressure for 8 minutes. Following this, the pattern in silicon dioxide is transferred to silicon by inductively coupled plasma (ICP) etch using HBr and Cl_2 at 400 W ICP power, 200 W RF power, 10 mTorr pressure and 20 Torr helium flow for backside cooling for 6.5 minutes. Finally, the chip is cleaned using Piranha for 15 minutes and followed with three cycles of Piranha/HF postprocess treatment as suggested from Ref. [5]. A schematic of the

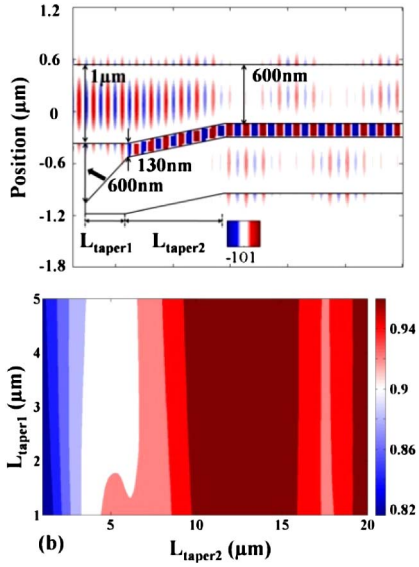

Fig. 2. (a) Simulated electric field for the mode converter. The simulation data show 98% conversion efficiency from strip waveguide mode to slot waveguide mode when $L_{\text{taper1}} = 4$ μm and $L_{\text{taper2}} = 10$ μm. (b) 2D plot showing simulated conversion efficiency as a function of L_{taper1} and L_{taper2}. The scale bar on the right indicates conversion efficiency.

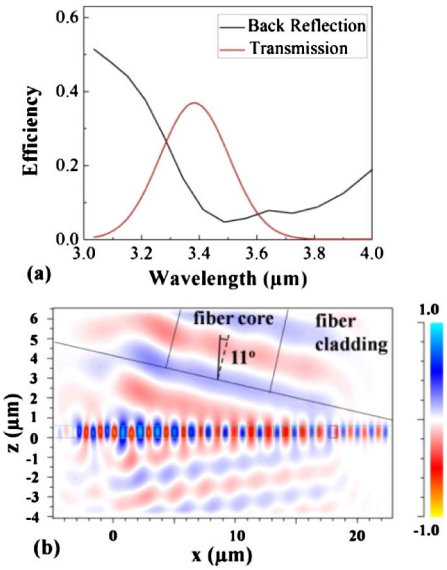

Fig. 3. (a) Simulated coupling efficiency from fiber (red curve) shows the peak is located around 3.4 μm, and the reflection (black curve) and (b) simulated output optical field from grating coupler to fiber.

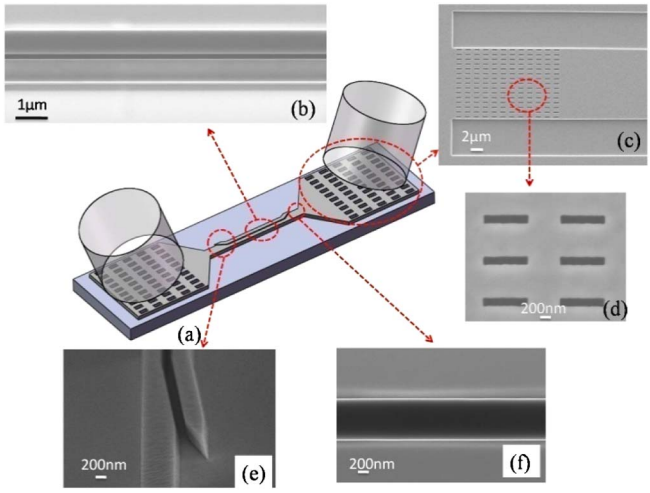

Fig. 4. (a) Schematic of the fabricated device, (b) SEM image of fabricated slot waveguide, (c) SEM image of SWG coupler, (d) magnified view of air holes, (e) close-up of strip waveguide to slot waveguide mode converter, and (f) SEM image of single mode strip waveguide with 1 μm width.

fabricated device is shown in Fig. 4(a). SEM images of the fabricated components are shown in Figs. 4(b)–4(f).

Devices are characterized using the setup schematically shown in Fig. 5. Light emitted from a continuous-wave interband cascade laser from Thorlabs, with a fixed wavelength of 3.4 μm, is passed through a pair of ZnSe lenses and coupled into a 9/125 μm single mode ZrF_4 optical fiber from Thorlabs. Light from the optical fiber is then coupled into the fabricated chip via SWG couplers. At the output end, another SWG coupler couples the light from chip to the output fiber. An InSb detector is used to measure the power from the output fiber. In order to improve the signal-to-noise ratio, a mechanical chopper is used with chopping frequency of 1 KHz, and the detected signals from InSb are demodulated by a lock-in amplifier.

In order to measure the coupling efficiency of the SWG couplers, light from the optical fiber positioned at 11° was coupled into an SWG coupler pair, and the power from another tilted output fiber was measured. An insertion loss of 10.8 dB was experimentally confirmed, which provides a coupling efficiency of 29% for each coupler, giving a discrepancy of about 7% between the measured and the calculated values. This discrepancy is caused

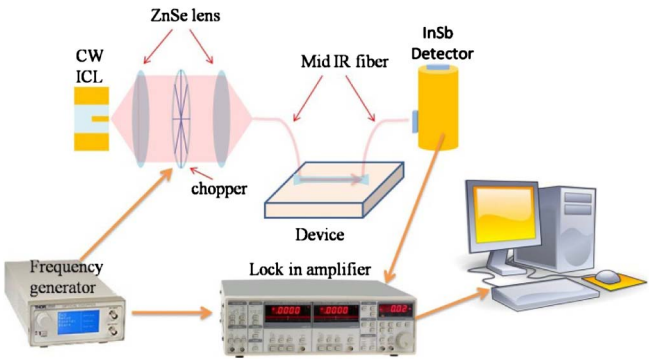

Fig. 5. Schematic of the experimental setup used to characterize our devices.

by fabrication-induced errors. We note that the input fiber is not polarization sensitive, hence we make the assumption that the input light is equally split between the two orthogonal TE and TM polarizations. However, the grating couplers have polarization selectivity between TE and TM of 18:1. Both ratios were included in the calculation of coupling efficiency of the propagating TE polarized slot mode. Coupling efficiency for different incident angles is also measured and compared with simulation results. Reasonable agreement between simulated and measured values is observed in Fig. 6.

The propagation losses of TE wave for the strip waveguides and the slot waveguides are measured using the cut-back method. Figure 7(a) shows the measured loss from eight strip waveguides with lengths ranging from 1 to 8 mm, and Fig. 7(b) shows four slot waveguides with length from 0.1 to 0.3 mm. By performing a linear fit to the data, we obtain propagation losses of 2.1 dB/cm and 11 dB/cm for the strip and slot waveguides, respectively. Since propagation loss of 0.74 dB/cm was observed in

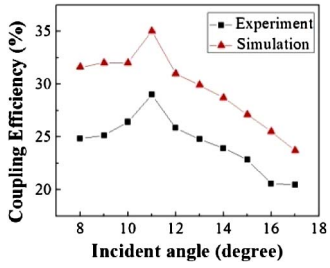

Fig. 6. Experimental measured and simulated coupling efficiency with different incident angles.

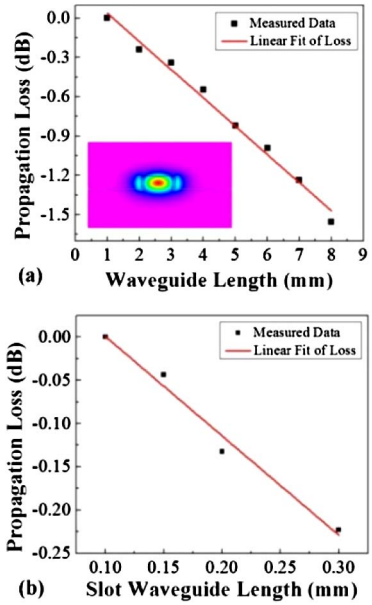

Fig. 7. (a) Measured loss of eight single mode waveguides fabricated on SOS operating at 3.4 μm wavelength. The waveguides are 0.6 μm in height and 1 μm in width. 2.1 dB/cm propagation loss is achieved by linear fitting. (b) Measured loss of eight slot waveguides fabricated on SOS operating at 3.4 μm wavelength. An 11 dB/cm propagation loss is achieved by linear fitting.

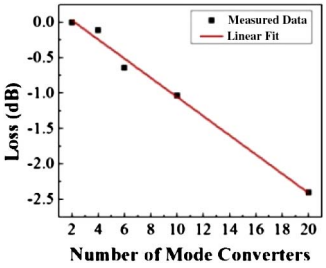

Fig. 8. Measured loss versus number of strip-to-slot waveguide mode converters at an operating wavelength of 3.4 μm. Approximately 0.13 dB loss per mode converter is measured, corresponding to 97% conversion efficiency.

SOS strip waveguide devices at 4.3–4.6 μm [5], the larger value can be attributed to increased Rayleigh scattering loss at shorter wavelength. Better control of device fabrication will lead to lower loss in our slot waveguides.

We also measured the conversion efficiency of our strip-to-slot waveguide mode converters by measuring the loss from several cascaded mode converters, as shown in Fig. 8. A linear fit to the data provides a loss of about 0.13 dB per mode converter, corresponding to 97% conversion efficiency, which agrees well with the simulated result of 98% in Fig. 2(b).

In summary, we demonstrate to our knowledge the first slot waveguides in SOS for TE polarized wave guiding at 3.4 μm wavelength. Coupling efficiency of 29% for SWG coupler is experimentally demonstrated. Propagation loss of 11 dB/cm was experimentally observed for slot waveguides. Two-stage taper strip-to-slot waveguide mode converters are utilized to gradually convert the strip waveguide mode into slot waveguide mode. The conversion efficiency for one mode converter is around −0.13 dB, corresponding to 97% conversion efficiency.

The authors acknowledge the NSF for supporting this work under grant no. IIP-1127251.

References

1. R. Soref, Nat. Photonics **4**, 495 (2010).
2. R. Soref, S. J. Emelett, and A. R. Buchwald, J. Opt. A **8**, 840 (2006).
3. Z. Cheng, X. Chen, C. Y. Wong, K. Xu, C. Fung, Y. Chen, and H. K. Tsang, IEEE Photon. J. **4**, 104 (2012).
4. T. Baehr-Jones, A. Spott, R. Ilic, A. Spott, B. Penkov, W. Asher, and M. Hochberg, Opt. Express **18**, 12127 (2010).
5. R. Shankar, I. Bulu, and M. Loncar, Appl. Phys. Lett. **102**, 051108 (2013).
6. F. Li, S. D. Jackson, C. Grillet, E. Magi, D. Hudson, S. J. Madden, Y. Moghe, C. O'Brien, A. Read, S. G. Duvall, P. Atanackovic, B. J. Eggleton, and D. J. Moss, Opt. Express **19**, 15212 (2011).
7. A. Spott, Y. Liu, T. Baehr-Jones, R. Ilic, and M. Hochberg, Appl. Phys. Lett. **97**, 213501 (2010).
8. C. Y. Wong, Z. Cheng, X. Chen, K. Xu, C. K. Y. Fung, Y. M. Chen, and H. K. Tsang, IEEE Photon. J. **4**, 1095 (2012).
9. V. R. Almeida, Q. Xu, C. A. Barrios, and M. Lipson, Opt. Lett. **29**, 1209 (2004).
10. Q. Xu, V. R. Almeida, R. R. Panepucci, and M. Lipson, Opt. Lett. **29**, 1626 (2004).
11. Z. Wang, N. Zhu, Y. Tang, L. Wosinski, D. Dai, and S. He, Opt. Lett. **34**, 1498 (2009).
12. Y. Liu, T. Baehr-Jones, J. Li, A. Pomerene, and M. Hochberg, IEEE Photon. Technol. Lett. **23**, 1496 (2011).
13. N.-N. Feng, R. Sun, L. C. Kimerling, and J. Michel, Opt. Lett. **32**, 1250 (2007).
14. C. Ma, Q. Zhang, and E. VanKeuren, J. Nanosci. Nanotechnol. **11**, 2524 (2011).
15. R. Palmer, L. Alloatti, D. Korn, W. Heni, P. C. Schindler, J. Bolten, M. Karl, M. Waldow, T. Wahlbrink, W. Freude, C. Koos, and J. Leuthold, IEEE Photon. J. **5**, 2200409 (2013).
16. X. Xu, H. Subbaraman, J. Covey, D. Kwong, A. Hosseini, and R. T. Chen, Appl. Phys. Lett. **101**, 031109 (2012).
17. Y. Zou, S. Chakravarty, D. Kwong, W. Lai, X. Xu, X. Lin, A. Hosseini, and R. T. Chen, IEEE J. Sel. Top. Quantum Electron. **20**, 1 (2014).
18. S. M. Rytov, Sov. Phys. JETP **2**, 466 (1956).